Aust. J. Phys., 1991, **44**, 397–419

Excitation of Swift Heavy Ions in Foil Targets. V* Production of Rydberg States

H. J. Hay and P. B. Treacy

Department of Nuclear Physics, Research School of Physical Sciences,
Australian National University, G.P.O. Box 4, Canberra, A.C.T. 2601, Australia.

Abstract

The results are summarised of previous experiments on the beam–foil excitation of Rydberg states of Br ions containing L vacancies. These show two populations, namely one with high angular momentum ℓ leading to 'yrast' cascades, and a separate low-ℓ population. Models for the production of such states in solid targets are discussed, and experiments to test the predictions of these models are described. The target-thickness dependence and downstream decay of the 'yrast' states is consistent with a standard charge-changing and capture model. The low-ℓ population is very sensitive to the presence of an applied electric field, and it is concluded that such Rydberg states are partly created by the radiative recapture of free 'convoy' electrons which travel physically near their host ions. Detailed level and decay schemes are described for the Br^{25+}, Ne-like system.

1. Introduction

In the previous publications I–IV (1983, 1986, 1987, 1988) we have reported on experiments to study radiation produced by decays of beam–foil excited ions of Br at 130 MeV. The radiations, comprising X-rays of energies between 1560 and 2725 keV, were shown to be the final transitions of cascading decays of Rydberg states. These states, as was shown by Lennard *et al.* (1972), consist of single-electron, high-n ($\gtrsim 10$) states based on screened ionic cores, and are Rydberg states, defined as hydrogenic states containing fractional principal quantum numbers $n^* = n - \mu_\ell$ in the notation of quantum-defect theory (Theodosiou *et al.* 1986). The post-target decays of such states was exploited in a number of studies (chiefly with single-electron ions) by H.-D. Betz and coworkers, both theoretically (Hasse *et al.* 1979) and experimentally (Betz *et al.* 1980), wherein the presence of yrast cascades, denoting states with high angular momenta ($\ell \lesssim 20\hbar$), was established. The presence of such 'large' ions was, and still remains, an intriguing problem.

The present work sets out to interpret the evidence that exists about the origin of beam–foil Rydberg states and to provide new relevant data. As a preliminary to this we summarise the evidence from our own work, which made use chiefly of decays into L vacancies in multi-electron ions: these

* Part I, *Aust. J. Phys.*, 1983, **36**, 7; II, 1986, **39**, 15; III, 1987, **40**, 12; IV, 1988, **41**, 681; V, Final Part.

0004-9506/91/040397$05.00

show enough complexity so that one can confidently infer the initial state populations from which they arise, and indicate possible mechanisms for their creation.

In Paper I, studies were concentrated on optical transitions in Cu ions, in the high-n ($\approx$20) region. It was demonstrated that yrast cascades do occur via transitions $(n, \ell = n-1)$, $(n-1, \ell-1)$, ... with the specific n and ℓ quantum numbers identified. Also, by studying the yrast sequence in targets of different thicknesses, it was shown that yields of such sequences increased with increasing target thicknesses. Such increased yields are not specifically charge- or n-dependent, and must be attributed to *preparation of the states via in-target processes.* They may be *created* at the target surface, as was postulated by many authors (Lennard and Cocke 1973), but must be prepared by processes occurring in the target bulk. Such a description applies rather similarly to the creation of 'convoy electrons' as was noted in I (cf. Breinig *et al.* 1982).

In Paper II, detailed studies were made of the distribution of 'downstream' X-rays generated by 130 MeV Br ions in Rydberg states with single L vacancies created by transmission through a 20 μg cm^{-2} carbon foil. These are 25^+, or Ne-like ions, whose decays correspond to the level scheme summarised in Appendix A on spectroscopy. There are decays seen at the bottom of the yrast sequence, but also two others specific to the L-vacancy regime (II, Table 1). These are:

(A) A sequence $n=3$ to $n=2$, comprising two distinct lines described as A1(3s–2p) and A2(3d–2p) transitions. These 1·5–1·7 keV X-rays are identified as the bottom steps from the yrast sequence; the presence of 3s electrons results from an explained trapping of substates at the 3d level. The degree of trapping into 3s states with spin–parity 1^-, which leads to the A1 group, is discussed in Appendix A of this paper. A side-product of the trapping is a related 2^- state, whose magnetic quadrupole decay is strongly inhibited. This survives downstream to produce the pure A1 X-ray, as was described in III.

(B) An $n=4$ to $n=2$ sequence at 2·0 keV identified as B(4d–2p) was observed; this is the expected low-intensity E2 ($\approx$5% of E1) crossover to the foot of the yrast sequence.

(C) The highest energy L X-ray observed, less intense (~4% of A) but distinct, of energy 2·7 keV. This is due to a direct-capture transition leading to the decay labelled C(ns–2p), with $n \gtrsim 10$. It is clearly distinguished from the lower energy X-rays, as well as from the radiative-capture X-ray at 3·5 keV (II, Fig. 1). Its presence denotes a population distinct from the main high-ℓ sequence, and demands a quite different creation mechanism.

In Paper III, an analysis was made of the populations of Rydberg states that could fit the time-dependent downstream decays observed in the beam–foil situation. This analysis comprised a Monte Carlo realisation of the decays of populations which had previously been described in an analytical simplification by Hasse *et al.* (1979). These calculations made certain assumptions as to the decay sequence of the hydrogen-like states involved; later work, to be described in detail in Appendix B, shows that this was justified. However,

the populations assumed in III were restricted to the two forms, namely a *statistical* one (on the yrast sequence)

$$\rho_s(n, \ell) = \frac{2\ell+1}{n^2} n^{-\beta_s} \tag{1a}$$

and a *direct* one

$$\rho_d(n, \ell{=}0) = n^{-\beta_d}. \tag{2a}$$

The naming of the distributions (1a) and (2a) should be regarded as descriptive, being based on their ℓ dependences as follows: ρ_ℓ (1a) is proportional to $2\ell+1$, which suggests a weighting of $\rho_\ell/(2\ell+1)$ per ℓ substate, i.e. that all the magnetic substates are of *statistical* weightings; ρ_d, on the other hand, contains only s-wave ($\ell = 0$) components, and such excited states are able to make *direct* decays to fill p vacancies. The reason why relatively high-ℓ states in (1a) can exist will be addressed later in a model (Section 2*a*), while pure s-states (2a) will be found to have more than one origin (Sections 2*b* and 2*c*). The mechanisms which will be described for the production of all these populations are different in time and space, hence they cannot interfere.

It turned out that excellent fits could be made using population indices (III, Table 2)

$$\beta_s = 2{\cdot}135 \pm 0{\cdot}035, \tag{1b}$$

$$\beta_d = 2{\cdot}38 \pm 0{\cdot}04 \tag{2b}$$

and intensities (summed over all $n \geq 3$) of 63% and 2·5% per 25^+ ion respectively. As was noted in III, such indices are difficult to reconcile with electron-capture mechanisms, which usually predict β values of 3, for n values $\gtrsim 5$ (Dubé and Salin 1987). It will be shown in Section 2*a* below that the populations (1) and (2) are unnecessarily restrictive. We shall, however, for definition, refer to them as the 'statistical' and 'direct' populations. Guided by a wish to fit our data with β values of 3 with a realistic production model, we have re-analysed all data. This is described in detail below.

The layout of this paper is as follows: Sections 2*a* and 2*b* discuss the origins of the statistical and direct populations and describe fits to data with population indices $\beta_s = \beta_d = 3$. The details of such fits are given in Appendix B. For describing the statistical distribution we rely on the work of Burgdörfer (1988), but the theory of the direct population is given in detail, being an expansion of the outline by Treacy and Hay (1988) in the same publication. The effects of the strong surface field on the emergent ions is discussed in Section 2*c*. In Sections 3*a* and 3*b* we describe some experiments undertaken to test the production models, and the conclusions are discussed in Section 4.

2. Models for Foil Excitation of Rydberg States

A hydrogenic atom with known n and ℓ quantum numbers has an average 'size' defined in terms of wavefunctions by a mean radial coordinate

$$r_{n\ell} = \frac{n^2 a_0}{Z}\left\{1 + \tfrac{1}{2}\left(1 - \frac{\ell(\ell+1)}{n^2}\right)\right\}, \tag{3}$$

where Z is its net core charge and a_0 the Bohr radius 0·529 Å. Its corresponding geometric mean free path in a solid is $(N\pi r_{n\ell}^2)^{-1}$, where N is the number density of valence electrons in the solid, which thus for Ne-like Br with $n=$ values 1, 10 and 100 in carbon is of order 1800, 18 and 0·18 Å respectively. For n values increasing from (say) to 100, the Rydberg states detected must be visualised as arising correspondingly nearer to the target's exit surface. As will be seen below, the properties and likely creation of the statistical and direct populations are very different, and will be considered in Sections 2*a* and 2*b* respectively.

(a) Statistical Population

A Monte Carlo computation has been made by Burgdörfer (1988) of the motion of an ion in a solid target. This used a classical Langevin equation of motion for a combined drift force and a fluctuating force, both constrained to predict elastic and inelastic electron (≈1 keV) mean free paths in accordance with known data (Koscher *et al.* 1984).

The picture emerges of an in-target ion exchanging electrons which may become bound in a state of n and ℓ values, then quickly pass through an unbound mode back to the original orbit; this orbit may be so short-lived that a distribution of states is generated. The tendency of an electron to remain near its bound orbit is enhanced by Coulomb focussing due to the ion, and reduced by 'Coulomb defocussing' due to scattering off target ions and their electrons. Burgdörfer reported that the calculations show a tendency to *trapping* of electrons in the presence of these forces, and this is proposed to justify the experimental observation that convoy electrons are observed (Sellin *et al.* 1986) to have mean free paths of an order of magnitude longer than do free electrons of the same energies in solid targets.

In order to predict the actual distribution in n and ℓ of electrons emerging from a target, it is necessary to assume the existence of a distribution of bound states, and follow the 'random walk' in ℓ values during the time the Coulomb focussing and trapping is occurring. *No numerical prediction of this has been published.* Qualitatively, one might expect initially:

(a) an n^{-3} dependent cross section for capture of electrons into n states (Dubé and Salin 1987).
(b) A fairly uniform initial distribution of ℓ substates. This is fairly evident in the continuum distorted-wave capture model (CDW) though not, we note, in the more primitive OBK model (Burgdörfer and Dubé 1985).
(c) Because of Coulomb trapping, a high retention of the initially-captured electrons in their original n state. It seems likely that passage through the target will tend to reduce the high-ℓ population via ℓ-mixing collisions (Hickman *et al.* 1983), leading to electrons with smaller transverse, or elliptical, orbit sizes, and consequently better transmission. A 'cut-off' ℓ distribution is thus to be expected.

As mentioned in Section 1, a fit to the time-dependent downstream decays of the A ('statistical') X-rays was made in Paper III with the corresponding population of equation (1b). We now discuss a fit with β_S equal to 3; numerical details have been separated out and are in Appendix B. It became evident that

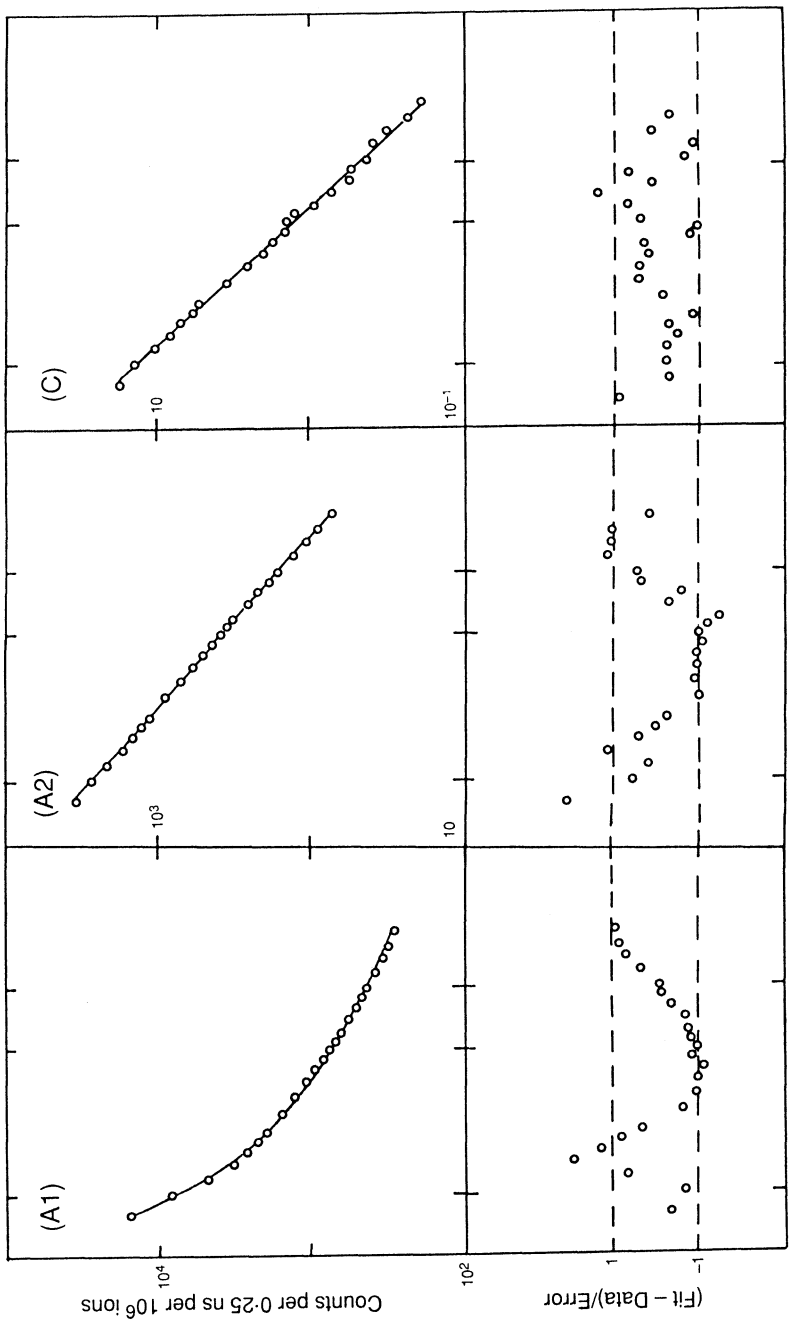

Fig. 1. Decays of X-rays detected downstream of a 20 μg cm^{-2} carbon target bombarded by a 130 MeV Br beam incident in a 10^+ charge state. The ordinates represent logarithms of decays per 0·25 ns interval and abscissae are logarithms of downstream distance in mm: (A1) A1 X-ray as defined in Section 1 from (3s–2p) transitions; (A2) A2 X-ray from (3d–2p) transitions (A_{23} of Paper III); (C) C X-ray as discussed in Section 2 from ns–2p with $n \gtrsim 10$. Deviations are represented in units of (±) standard errors, shown as dashed lines, in the boxes below the labelled graphs. Within statistics, these are not significantly different from the fits of Paper III, Figs 2 and 3.

the data require a reduced high-ℓ population ($< n-1$), and we tried using two forms. The first was

$$\rho_s(n, \ell) = \left(\frac{2\ell+1}{2(\ell_{max}+1)^2}\right) n^{-3}, \tag{4a}$$

where ℓ_{max} is equal to $n-1$ for $n < n_{cut}$ and is assumed to fall off exponentially for n greater. The relation between ℓ_{max} and n is displayed in Appendix B in Fig. 8. An alternative form tried with a less abrupt change of population at ℓ_{max} was

$$\rho_s(n, \ell) = \left(\frac{1}{\ell_{max}+1}\right) n^{-3}. \tag{4b}$$

The difference between the forms (4a) and (4b) is clearly that the former gives equal weights to all substates for ℓ values between $\pm\ell_{max}$, while the latter weights all ℓ values equally. The form (4b) is probably the more consistent with our remarks above that only the most elliptical are stable orbits; however, no really satisfactory fit to the data was found with it.

The results of the fits, including small (≈1%) contributions from components needed to account for the 'C' X-rays (Sections 2*b* and 2*c* below), are shown for all A X-rays in Fig. 1 (A1) and (A2). It must be stressed that there are some free parameters, as discussed in Sections 2*b* and 2*c*. The fits lie reasonably within statistical errors, as illustrated by the deviations depicted below the plotted points. There are contributions to the A X-rays from 25^+ (Ne-like) and 26^+ (F-like) ions, which exist in a known proportion. The three fitted parameters defining ℓ_{max} are defined explicitly in Appendix B. These are, of course, completely free parameters insofar as the 'statistical' population emerging from the target is not directly measurable.

(b) Direct Population

As shown in Paper III, there is a distinct low angular-momentum population ρ_d, equation (2a), responsible for the direct 'C' X-rays. An origin for this quite separate from that of the statistical population must be assumed. A possible mechanism is the capture, at or near the target back surface, of convoy electrons; that is, electrons travelling close in velocity and position to the ions, generated mainly by projectile ionisation, or 'electron loss to the continuum' (ELC). This was proposed by Treacy and Hay (1988), and a numerical calculation of the Rydberg population developed from this will now be summarised. One must first know N_e, the number of unscattered ELC electrons produced per ion, exiting each target thickness. This was obtained from fits to data on charge fractions of 130 MeV Br ions (Pender and Hay 1983) using a Monte Carlo simulation like one already used for 105 MeV Cl ions (Hay *et al.* 1984). The number of unscattered ELC electrons ejected depends on the electron's attenuation length as deduced, for example, by Powell (1974). In Fig. 2*a* we plot values of N_e (dashed curve), together with the measured 26^+ charge fraction, on which most of the capture yield should be dependent.

In order to know the probability of electron capture, it is necessary to assume a suitable electron capture mechanism. If this occurs post-target, it

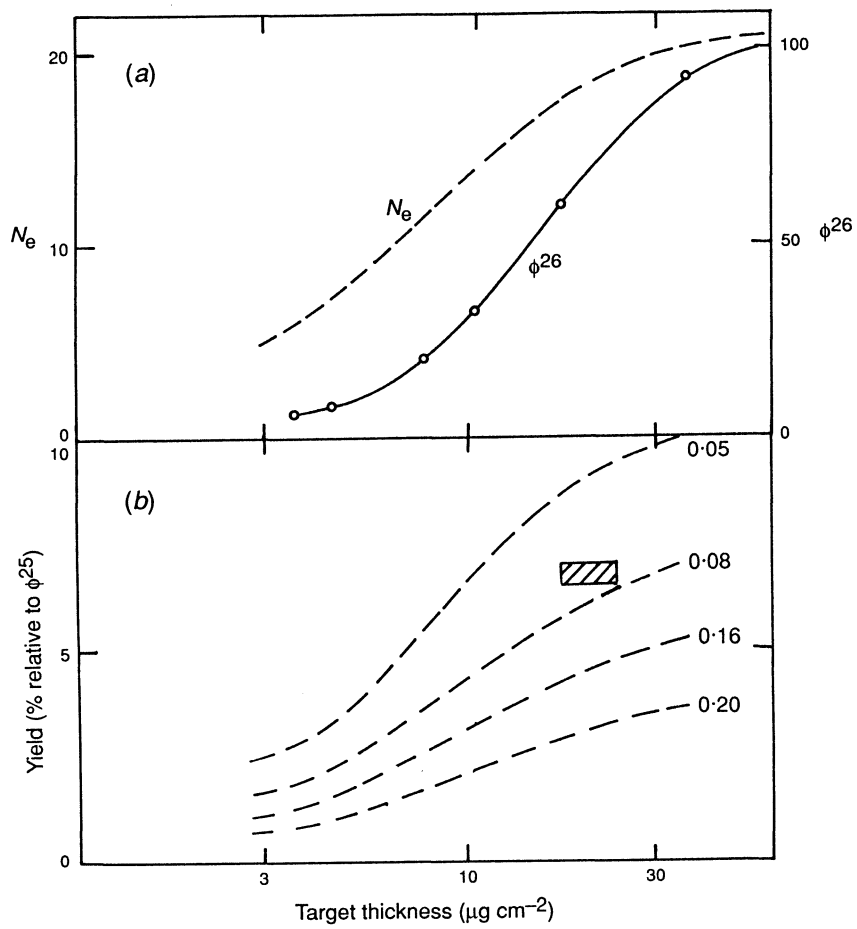

Fig. 2. Target-thickness dependence of quantities connected with the C X-ray yield from an incident 10^+ charge state 130 MeV Br beam: (*a*) Dashed curve N_e: the number of ELC electrons in-target per ion, deduced from a fitted charge-state distribution. Full curve ϕ^{26}; the emerging 26^+ charge-state fraction. (*b*) Dashed curves: predicted REC yields of 25^+ Rydberg ions from capture of ELC electrons, for incident bound radii between 0·05–0·2 Å. Shaded box: yield with errors corresponding to the observed REC component of the X-rays.

must comprise two-body radiative electron capture (REC), the cross section for which may be written (Bethe and Salpeter 1957)

$$\sigma = 1 \cdot 05 \times 10^{-22} (Z v_0 / v)^2 \sum \rho_n / n^3 . \qquad (5)$$

Here σ is in cm^2, Z is the effective charge of the ions, and v_0 and v are respectively the first Bohr velocity and the captured electron velocity (in the ion's centre-of-mass frame); ρ_n is the effective number of electron vacancies for the nth shell; we shall see below that $\rho_n \leq 2$. The ELC velocity v may be obtained from the Born theory (Drepper and Briggs 1976) and is approximated here by the exponential distribution $\exp(-11 \cdot 7v/u)$, where u is the Br beam velocity and $v \leq 2u$. It remains to use (5) in a way that recognises that the electrons are liberated out of a confined region. Since they arise chiefly from

ionisation of the L and M shells, they are expected to be confined initially within an r.m.s. radius in relation to their original host ions given by (3). For a Br ion in carbon the values are 0·07 and 0·2 Å for the screened L and M shells, with the lower value expected to be favoured (Pender and Hay 1983).

From now on, let us presume that the ELC electrons are sufficiently close to their host ions so that recapture to these is enhanced. The use of a time-dependent confinement volume necessitates a departure from the usual practice of assuming a constant density of 'targets' (ions), which is to be replaced by a density of one per electron-occupation volume. A natural way to compute such a volume is furnished by elementary path-integral theory (Feynman and Hibbs 1965). Let us assume that a free electron exits the target and becomes exposed to the full ionic potential. Great convenience, and some physical justification, comes from assuming that it exists initially in a wave packet with a radial function (Edwards and Gulyaev 1964) which is gaussian. For a free particle, the wave packet may be shown (Feynman and Hibbs 1965; p. 51 equation 3-29) to remain gaussian and expand in time with a width $b(t)$ given by

$$b^2(t) = (a + vt)^2 + (wt)^2 , \tag{6}$$

where $w = \hbar/ma$ is its uncertainty of velocity due to the initial confinement radius a. Using equations (5) and (6) it is not difficult to show that the probability $P(t)$ that electron capture has *not* occurred by time t is given by

$$P(t) = \exp\left\{-c\left(\frac{Vt + ar}{[a^2(1-r^2) + (Vt + ar)^2]^{1/2}} - r\right)\right\}, \tag{7a}$$

where

$$c = \frac{N_e\, \sigma}{\frac{4}{3}\pi a^2 (1 - r^2)}, \tag{7b}$$

$$V = (v^2 + w^2)^{1/2} , \tag{7c}$$

and $r = v/V$. Typically, with the mean value of $v = 0{\cdot}085u$ and both u and V of order 1 cm ns^{-1}, r is less than 0·1. In writing equation (5) it had already been anticipated that v/Zv_0 is also small ($\approx 0{\cdot}3/Z$ with $Z \approx 25$).

Equation (7a) applies to the expansion of a free-particle wave packet. Though there is a strong Coulomb distortion in the post-target area, expansion remains dominated by the velocity uncertainty w rather than the Coulomb-modified value, for the range of values of a employed here. These velocities depend respectively on a as $a^{-1/2}$, so the Coulomb effect is relatively less at *small* distances.

The probability $P(t)$ is exponentially decaying for small t, but for large t it approaches an asymptotic or 'hard core' value which, for small r, becomes simply $\exp(-c)$. For the present problem the probability of single capture, $1 - P(\infty)$, is around 0·005 which illustrates that the cross section for REC, equation (5), is small by atomic standards. The yield R of Rydberg states was calculated by a Monte Carlo method in a time sequence, using the assumed initial number N_e of electrons available for capture. The results are displayed in

Fig. 2*b* for values of a within the reasonable outside limits 0·05–0·2 Å. These calculations include the effect of capture by the calculated amount of 27^+ and 28^+ charge fractions which leads to the observed 26 : 25 and 27 : 26 fractions of 0·218 and 0·165. The shaded rectangle at the value $a = 0{\cdot}08$ and 20 μg cm^{-2} corresponds to the fit of data in Fig. 1. The population predicted from the REC model, equation (5), is of the standard n^{-3} form, which implies a time-decay index (Hasse *et al.* 1979) α of 1·67, compared with the experimental value (Treacy and Hay 1988) of 1·46±0·03.

In the calculations described above, it was assumed that electrons may be captured to form only s-wave bound states, and hence a solely s-wave Rydberg population. In the experiment (Paper II) such states were observed decaying by filling of 2p vacancies in the 25^+, 26^+, ... charge states that had such vacancies. As explained above, there is no evidence for ℓ values greater than 2 in the direct population, although REC does not favour low angular momentum capture of free electrons (Burgess 1964). However, the multipole contributions of high ℓ to the ELC electrons have been measured (Berry *et al.* 1986) to show that $\ell > 2$ carried typically $< 7\%$ of the intensity; $\ell = 2$ is around 20% and its neglect here does not significantly affect the calculation. As a consequence, the maximum value of each ρ_n is two, i.e. the number of s-wave states per shell. This limitation arises because REC is a radiative process involving overwhelming dipole transitions. Other theories (Day and Ebel 1979; Seideman *et al.* 1987), which assume that the connection between bound and free states is made not by a dipole transition but by an 'overlap integral', would not predict the apparent preponderance of final-s states.

The model presented here assumes that electrons are captured from a radius comparable with that at which they were ionised (~0·1 Å) after traversal of up to the attenuation length (~30 Å). There is other experimental evidence (Sellin *et al.* 1986) that ELC electrons do have enhanced free paths in solids, and this has been described as due to 'Coulomb focussing ... redirecting electron motion along the favoured direction'. The more detailed theoretical picture of Burgdörfer (1988) reveals that a consequence of this is an enhanced probability of ELC electrons to be near their host ions after traversal of solids.

In summary, there is some evidence that a direct Rydberg population, as studied by L X-rays following beam–foil excitation of 130 MeV br ions, may be created by post-target capture of ELC electrons which emerge in close proximity with their host ions. This model predicts that the target-thickness dependence of the (25^+) direct Rydberg population should follow fairly closely that of the 26^+ charge fraction. It does appear that the predicted intensity is too low, and that its population index is not in agreement with the data, so that a further source of 'C' X-rays must exist.

(c) Effects of the Target Surface Region

It is commonly recognised that the state of an ion emerging through the surface of a solid target is subject to strong perturbing electrostatic forces, essentially the fields due to energy loss. For 130 MeV Br ions in carbon, these are of order 10^9 V cm^{-1}. Burgdörfer and Dubé (1985) did classical computations using a post-collision-interaction (PCI) model which involves mixing of Stark states via the Coulomb electron–target interaction, and predicted a significant

mixing of ℓ substates. In the case of an ion exiting a target, it is necessary to model the ion–surface potential decreasing from the 'dE/dx' field to zero, and use this to compute the transitions induced by it among the actual ($n\ell m$) states. This process may be described quantum mechanically by means of the Landau–Zener effect (Landau and Lifshitz 1977). Specifically, the probability of anti-crossings between levels of a Rydberg ion in a strong electric field has been described in detail by Komarov *et al.* (1980). They show that two Stark levels, designated by parabolic quantum numbers (n, n_1, n_2, $|\, m\,|$), whose asymptotic trajectories appear to meet at a certain field, have a finite probability of *avoiding* crossing and thus effectively exchanging quantum numbers. The degree to which avoidance is possible is governed by the magnitude of the ion's quantum defect μ_ℓ which tends to vanish for $\ell \gtrsim 2$ (Theodosiou *et al.* 1986). Not only will a low-ℓ Rydberg population index β_d be thereby altered, but it must be expected that electrons from inner (1s, 2s, 2p) cores will be excited, thus yielding a third independent Rydberg population. These effects will now be discussed.*

An ion emerging from a solid target in a state ($n\ell m$) must be visualised as being in a superposition of parabolic states (n, n_1, n_2, $|\, m\,|$), subject to a fluctuating electric field F, with rate-of-change dF/dt due to the energy loss, or dE/dx force, of order 10^9 V cm^{-1}. As shown by Komarov *et al.* (1980), when the ion's energy $E_i(n,\ n_1,\ n_2,\ |\, m\,|)$ approaches that of another (unoccupied) level $E_j(n',\ n_1',\ n_2',\ |\, m\,|)$ the probability that a transition occurs between the levels is given by

$$W_{ij} = \exp\,(-\xi_{ij}), \tag{8a}$$

where

$$\xi_{ij} = \frac{\pi}{\hbar}(\Delta E_{ij})^2 \left(Z \left| \frac{\partial E_i}{\partial F} - \frac{\partial E_j}{\partial F} \right| \frac{\mathrm{d}F}{\mathrm{d}t} \right)^{-1}. \tag{8b}$$

In (8b) ΔE_{ij} is given by the closest adiabatic spacing of the levels E_i, E_j:

$$\Delta E_{ij} = 2(nn')^{-3/2} \sum_{\ell \gtrsim |m|} (KKk_1\ k_2 \,|\ell|\, m\,|)(K'K'k_1'k_2' \,|\ell|\, m\,|)\mu_\ell, \tag{8c}$$

where $K = (n-1)/2$, $k_1 = (|\, m\,| + n_1 - n_2)/2$, $k_2 = (|\, m\,| - n_1 + n_2)/2$ and similarly for K'. Note that for hydrogenic levels we have $\mu_\ell = 0$ and the crossing probability is unity, so no interchange of quantum numbers may occur. In (8c) the $(KKk_1\ k_2 \,|\ell|\, m\,|)$ are Clebsch–Gordan coefficients.

The equations (8) were programmed for the electric field at the exit of the target by assuming that the ion is exposed to the 'dE/dx' field (3×10^9 V cm^{-1} for Br in carbon), which was assumed to be generated by a three-dimensional Born–Mayer or a Molière potential (Torrens 1972) decreasing from its maximum value to zero as the ion exited from the target. Using (8a) it was then possible to compute absolutely the probability $\Sigma_j(1 - W_{ij})$ that for level 'i' anti-crossing

* In an earlier work (Hay and Treacy 1990) the promotion effects on the direct population alone was studied. The present work thus generalises the viewpoint.

occurs. (This is typically small, $\approx 10^{-4}$.)* The low-ℓ (<2) population includes the (n^{-3}) population distribution resulting from the radiative-capture mechanism discussed in Section 2*b* above, to which is added the (100% per ion) population from nine inner electrons of the Ne-like ion's core. All these electrons must be considered subject to the Landau–Zener promotion process. In Fig. 3 we show the resulting calculated population, which now includes contributions from the (6%) n^{-3} 'REC' population, and the (100%) core $1s^2 3s^2 2p^5$ electrons. The result is in fact consistent with an $n^{-\beta}$ population with β near 2·4 (shown dotted), and this agrees with the work of Paper III which found a fit to the data with $\beta_d = 2 \cdot 38$ (equation 2b). As mentioned in Section 2*a*, the task of fitting a population to an observed downstream decay is discussed in Appendix B.

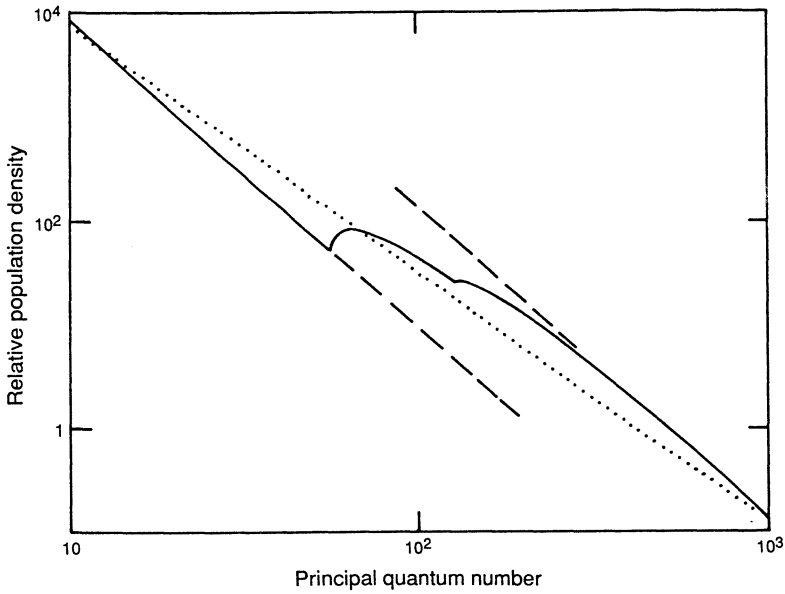

Fig. 3. Calculated initial population of low-ℓ Rydberg states. The n^{-3} contribution from REC is seen at top left, and the two 'bumps' rising at n values near 50 and 100 are from Landau–Zener promotion at the target surface of bound $n = 2$ and $n = 1$ electrons respectively. The dotted line represents the power law $n^{-2 \cdot 4}$, which was used in Paper III to fit the observed downstream decay of the C X-ray.

The Landau–Zener process must be considered as able to modify the s-wave parts of both the Rydberg population and of all the inner-shell electrons. In Fig. 1 (C) a satisfactory fit is shown to the downstream decays leading to 'C' X-rays subject to that process. The result is in fact quite similar to the fit already proposed with an initial $n^{-\beta}$ population with $\beta = 2 \cdot 4$ (Paper III). The fit in Fig. 1 (C) is not linear but deviates from a power law by a few per cent. As in Fig. 1 (A1) and (A2), the deviations between fits and data lie within expected experimental errors.

* Such low probabilities result in trivial contributions from sequences of two or more anti-crossings, and also negligible amounts from the 'statistical' states, compared with promotion from the inner shells. The time scale is such that REC has not yet occurred.

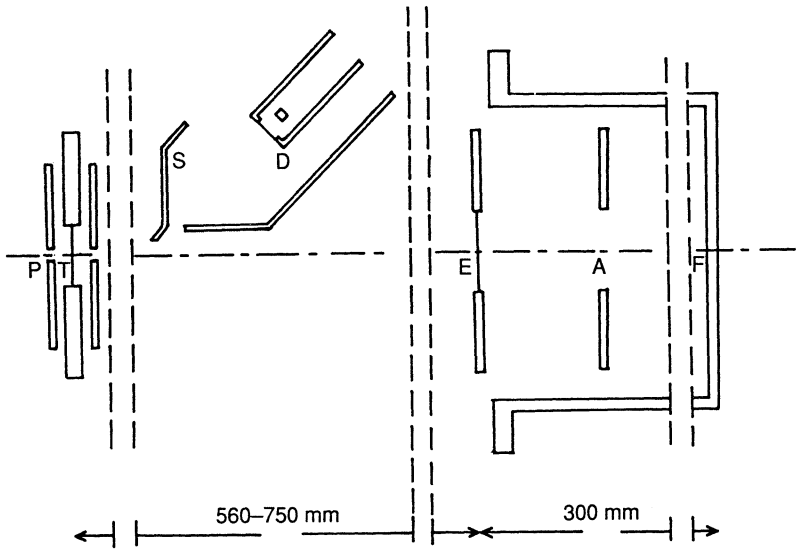

Fig. 4. Schematic illustration in elevation of (*left*) target and detector geometry with applied electric field and (*right*) Faraday cup to detect ion current irrespective of incident ion beam charge state. Symbols represent the following (left to right): P electrostatic plates; T foil target; S detector shield; D detector; E equilibrator foil; A anti-secondary electrode; F Faraday cup. The horizontal scale is indicated by dimensions in mm, with dashed lines (three sets) implying breaks of distance. The scale of dimensions are: beam diameter 2 mm, target-field gaps 6 mm, field plate aperture 3 mm, Faraday cup aperture 25 mm and cup diameter 100 mm. The target and plates can be moved along the beam axis.

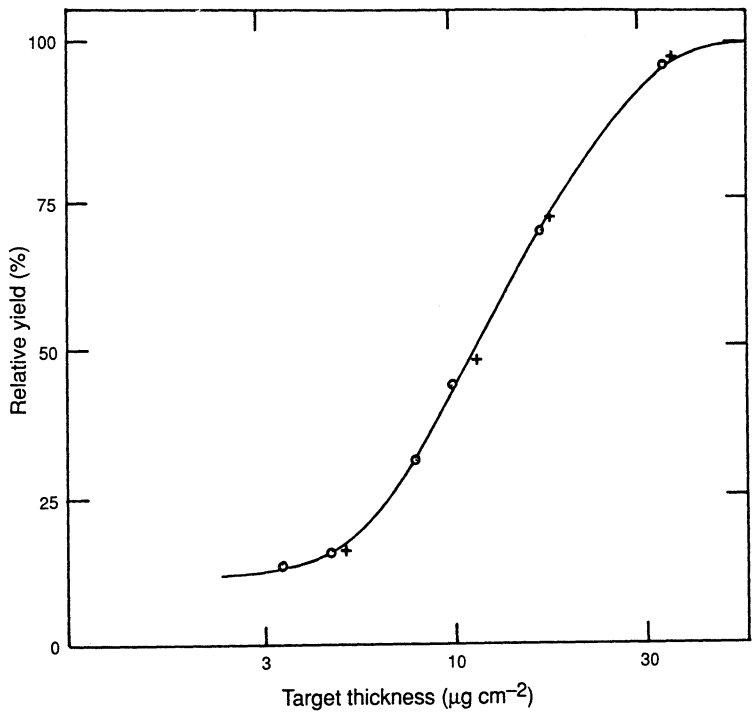

Fig. 5. Comparison of target-thickness dependence of X-ray yield and the total L-shell vacancy-state ion yield. The circles and eyeball-fitted curve represent the measured charge fraction corresponding to ϕ (equation 9), while the crosses display the X-ray yield detected at a point 30 mm downstream of the target.

3. Experiments to Test Production Models

In Section 1 evidence was described which shows that Rydberg ion yields increase with target thickness, thus ruling out a pure back-surface capture mechanism. The relative yield of X-rays to their charge-state fractions is obviously of importance to compare to a production mechanism such as that of Burgdörfer (1988). Such measurements are described in Section 3*a* below. To test the possible validity of the radiative-capture model described in Section 2 (Treacy and Hay 1988), other experiments have been done to determine the effects on the beam–foil X-rays of an applied external field. These are described in Section 3*b*.

(a) Target Thickness Dependence of Yields

It was decided to measure the yield of X-rays from recoiling ions at a fixed point downstream from targets of different thicknesses. This entailed a knowledge of the beam intensity irrespective of its charge state, which depends on the target used. For this purpose, a Faraday cup was constructed as shown in Fig. 4. By means of this, it was possible to measure the charge collected from a beam which had been charge-equilibrated *after* detection of the radiation, with full suppression of the secondary electrons liberated from the equilibrating foil.

The yield of all L X-rays, normalised to the beam particle intensity, is plotted in Fig. 5. Also plotted in Fig. 5 is the measured sum of charge fractions:

$$\phi = \sum_{q \geq 25} \phi^{(q)} \tag{9}$$

which, having L vacancies, are capable of generating L X-rays. For the X-ray measurements the beam of 130 MeV Br ions was pre-equilibrated by passing through an 88 μg cm^{-2} carbon foil. In this process, the ions' energies were degraded to 125·8 MeV. The charge-state data are for the same beam, although the original data from which they were obtained were measured with separated charge states and a 130 MeV beam. The plotted points were adjusted for the reduced beam energy by using the empirical form of Baudinet-Robinet (1981) to extrapolate the measured distribution from a higher beam energy. Because an equilibrator foil was used, which impaired the beam's focal quality, no attempt was made in the data of Fig. 5 to separate out the X-ray energies. Because the majority of X-rays are 'statistical' (A1 and A2) (Section 2) with less than one per cent from the low-ℓ 'direct' (C) distribution, the result in Fig. 5, that the X-rays closely follow the sum of charge fractions, may be interpreted to say that the majority of Rydberg states are present in proportion to the charge fractions.

The X-ray yields in Fig. 5, for lower target thicknesses ($\lesssim$10 μg cm^{-2}) actually fall below ϕ (equation 9), as indeed is to be expected on the basis of the data of Paper I and the expectation that the Burgdörfer mechanism 'builds up' as the ion traverses the target.

(b) Dependence of X-ray Yield on an Applied External Field

The model proposed in Section 2*b* is that a substantial part of the C X-rays result from a Rydberg population formed by capture of free electrons. Such a

distribution should be susceptible to the influence of a relatively weak electric field, much smaller than that necessary to cause Stark quenching (as will be discussed below). The relative effect of such a field on the A and C X-rays should therefore be of interest for the model proposed. To study this, a region of the downstream path of the beam was exposed to a constant electric field directed axially along the beam direction, by the apparatus shown schematically in Fig. 4. The symmetrical field arrangement shown was necessary in order to protect the thin carbon target foil from strong electrostatic forces. The beam entered and escaped from the field region by a small 'immersion' hole which did not cause significant field distortion in the region (±5 mm) surrounding the target.

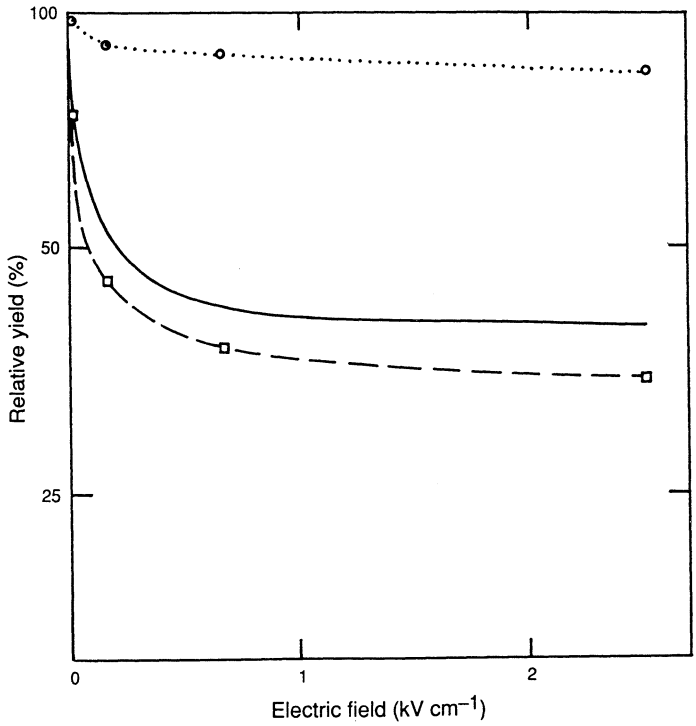

Fig. 6. Effect of an axial electric field in quenching X-ray yields at 30 mm from the target. The circles and dotted curve represent the summed A X-ray; the squares and dashed curve represent the C X-ray. The full curve is a plot of the C-to-A ratio, as discussed in the text.

X-ray yields were measured at a distance of 30 mm downstream from the target, and the results are plotted in Fig. 6 as a function of the applied field. For fields $\gtrsim 2$ kV cm^{-1} a small ($\approx 10\%$) attenuation was detected in the A X-ray, while a much greater (70%) reduction was made in the C: surprisingly, a field of $0 \cdot 1$ kV cm^{-1} was sufficient to reduce the C intensity to half. To interpret these attenuations, it is first necessary to consider the possible effect of Stark quenching, which is the predissociation of bound levels by an external field. Detailed calculations for hydrogenic levels (Damburg and Kolosov 1979) show that this effect is totally unimportant for the states with n values from 30 to 300 decaying to form the C X-rays.

A more direct interpretation of the large observed attenuation follows from a consideration of the model for formation of the direct population (Section 3*b*). Referring to (7a), the initial time dependence of $P(t)$ may be visualised as exponential with a mean life of

$$\tau = \frac{a}{cV} = \frac{\frac{4}{3}\pi a^3}{N_e \sigma V} \qquad (Vt \ll a), \tag{10}$$

where the cross section σ, given by equation (5), is inversely proportional to n^3. With appropriate values of a, N_e and V, equation (10) leads to a value $\tau \approx 1 \cdot 6 \times 10^{-17}\, n^3$ s. The radiative capture process is perturbed by any field which can cause a free electron to drift by a distance comparable with the initial confinement $a \approx 10^{-9}$ cm of the wave packet. So the lowest n value for which this can happen is governed by the condition

$$a = \tfrac{1}{2} f \tau^2 \approx 2 \times 10^{-16}\, n^6, \tag{11}$$

where $f = e\epsilon/m$ is the acceleration of an electron (e, m) in a field ϵ, and τ is given above. This is satisfied by $n \geq 20$ and so the extreme attenuation of the C X-rays is understandable. In fact, the smallness of the radiative capture cross section σ ensures that the capture time τ is long, approaching several nanoseconds for $n = 150$, which is in the middle of the range of values contributing in Fig. 6.

Returning to the attenuations due to fields in the A X-ray, we see that these must be attributable to some extent to beam-deflection effects in the 'tight' geometry of Fig. 4, and for this reason the *relative* C : A attenuation is plotted in Fig. 6. This falls by 60% and, if our interpretation above is correct, this should be the proportion of REC X-rays in the spectrum. For the point 30 mm downstream at which the applied-field measurement was made, the fit (as described in Appendix B) predicts this to be 50%. Since both the results of Fig. 6 (60%) and this prediction (50%) are subject to an error of around 10%, the predicted content of 'REC C X-rays' is satisfactorily confirmed by the field-quenching results obtained.

4. Discussion

One of the most remarkable effects of the passage of swift ions through foil targets is the emergence of a prolific yield of Rydberg states of ions with significant high-n populations and high angular momenta ($\sim 1/n^3$, $\ell < 30$). Our data in Fig. 1 (A1) and (A2) confirm this. The description of Burgdörfer (1988) in terms of Coulomb focussing and trapping gives some insight on the observations, but from the energy-loss point of view the survival of high $(n\ell)$ states in a solid target remains surprising. The fits to our data suggest an n dependence of maximum ℓ cut down in the way illustrated in Fig. 8.

In our earlier work (II, III) we showed that study of L X-ray beam–foil spectra confirmed the existence of the high $(n\ell)$ or 'statistical' distribution which leads to the well-known yrast cascade terminating in 3d–2p (A2) and 3s–2p (A1) X-rays; the 3s level is fed via yrast blocking due to the availability of only a limited number of final 2p vacancy substates, thus forming a large number of $J^\pi = 2^-$ metastable 3s states of lifetime 800 ns (see Appendix B). In the

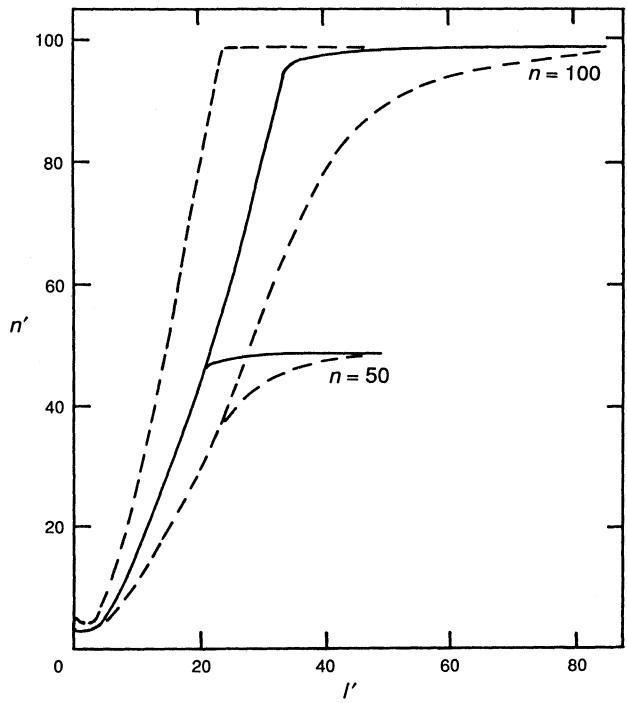

Fig. 7. Illustration of the branching of $(n\ell)$ hydrogenic states by electric dipole radiation according to the Gordon formula. The relative branching ratios to states $(n', \ell \pm 1)$ for labelled initial n values of 50 and 100 are shown by full curves (most probable) and dashed curves (50% of most probable) in the (n', ℓ') space.

present work we have shown that the 'statistical' distribution may originate from an initial $1/n^3$ population which decays preferentially by the above-yrast cascade route illustrated in Fig. 7; it includes the yrast cascade as a highest-ℓ component.

The L X-rays also have revealed the presence of a distinct 'direct' population of mainly s states which can decay directly to the ground state via the ns–2p or C X-ray. In the more usual studies of K X-rays in one- or two-electron ions, where the cascades end in a 1s vacancy, the 'direct' decays have not been noticed; not only will they be weaker but also their ns–2p energy is smaller, rather than larger, than that of the dominant X-rays.

The main effort of the present work, presented in Section 2, has been to advance physical reasons for the existence of a direct population, with quantitative fits to the C X-ray strength observed. Only about 30% of the C X-ray intensity of Fig. 1 (C) comes from the cascading down of the statistical population which initially comprises some 95% of the excited ions. In addition to the $\ell = 0$ part of the original statistical distribution, we have predicted that two other processes are capable of generating the direct population, namely post-foil capture of pre-liberated electrons (ELC), and foil-exit excitation of core electrons in the emerging ions (Stark mixing).

The former process occurs via radiative electron capture (REC), and the reason for a strong $\ell = 0$ predominance lies in the physical closeness of the

ELC electrons to their host ions, with a high probability of recapture even via the weak REC process. The proposal that ions lose then recapture the *same* electron receives confirmation from the effect, illustrated in Fig. 5, of externally applied electric fields which are too small to affect bound states. Because of the slow REC process, a relatively weak (~ 100 eV cm^{-1}) field can apparently 'sweep' an ELC electron from the grasp of its parent ion, irrespective of its direction of travel—unlike the situation in the Stark effect, so graphically described by Condon and Shortley (1951, p. 409). Both the REC probability and the degree of field quenching are quantitatively consistent with the observations.

The foil-exit excitation, generated via the well-known Landau–Zener anti-crossing mechanism, is explained in terms of Stark levels excited by the rapid fall of the strong electric field existing until the last atomic layer of the target. In Fig. 1 (C), the fitted contributions of C X-rays due to statistical, REC and Landau–Zener decays are, as percentages, 30 : 55 : 15 respectively. It is worth noting that the fraction of ions produced by Stark mixing is about 5 in 10^4; this is a typical proportion of high-n Rydberg ions measured by field-ionisation techniques (Vager *et al.* 1982). Those promoted to $n > 200$ asymptote to a $1/n^3$ distribution (Fig. 3); this too is consistent with field-ionisation estimates.

Summarising, the conclusion of this work is that the production of beam–foil Rydberg states, their decay intensities in the beam–foil region, and their response to external electric fields, are well described in terms of standard atomic capture, loss and excitation processes. The models used, as described in Section 2, depend on specific solid-state effects for the formation of both the observed populations of Rydberg states.

Acknowledgments

This paper concludes the work of the Atomic Collisions group in the ANU Department of Nuclear Physics. This has concentrated chiefly on excitations in the hitherto unexplored L-shell which has revealed an unexpected richness in the populations of Rydberg states. The present authors sincerely thank our Nuclear Physics colleagues for their toleration, helpfulness and friendliness towards projects which they surely must have wished were oriented to the nucleus rather than to outer-shell electrons. We also express our gratitude to our fellow collaborators over the past ten years: Ralph Alexander, Lynn Bridwell, Gregory Clark, Albert Muggleton, Charles Newton, John Söderbaum, Carl Sofield, and most particularly to Lindsay Pender.

References

Baudinet-Robinet, Y. (1981). *Nucl. Instrum. Methods* **190**, 197.
Berry, S. D., Elston, B. B., Sellin, I. A., Breinig, M., De Serio, R., Gonzales-Lepera, C. E., and Liljeby, L. L. (1986). *J. Phys.* B **19**, L149.
Bethe, H. A., and Salpeter, E. E. (1957). 'Quantum Mechanics of One and Two Electron Atoms' (Springer: Berlin).
Betz, H.-D. Rothermel, J., and Bell, F. (1980). *Nucl. Instrum. Methods* **170**, 243.
Breinig, M., *et al.* (1982). *Phys. Rev.* A **25**, 3015.
Burgdörfer, J. (1988). 'Lecture Notes in Physics', Vol. 294, p. 344 (Springer: Berlin).
Burgdörfer, J., and Dubé, L. J. (1985). *Phys. Rev.* A **31**, 634.
Burgess, A. (1964). *Mem. R. Astron. Soc.* **69**, 1.
Condon, E. U., and Shortley, G. H. (1951). 'Theory of Atomic Spectra' (Cambridge Univ. Press).
Damburg, R. J., and Kolosov, V. V. (1979). *J. Phys.* B **12**, 2637.

Day, M., and Ebel, M. (1979). *Phys. Rev.* B **19**, 3434.
Drepper, F., and Briggs, J. S. (1976). *J. Phys.* B **9**, 2063.
Dubé, L. J., and Salin, A. (1987). *J. Phys.* B **20**, L499.
Edwards, S. F., and Gulyaev, Y. V. (1964). *Proc. R. Soc. London* A **279**, 229.
Feynman, R. P., and Hibbs, A. R. (1965). 'Quantum Mechanics and Path Integrals' (McGraw–Hill: New York).
Gordon, W. (1929). *Ann. d. Phys.* **2**, 1031.
Hasse, R. W., Betz, H.-D., and Bell, F. (1979). *J. Phys.* B **12**, L711.
Hay, H. J., Pender, L. F., and Treacy, P. B. (1984). *Nucl. Instrum. Methods* B **2**, 505.
Hay, H. J., and Treacy, P. B. (1990). *Nucl. Instrum. Methods* B **48**, 107.
Hickman, A. P., Olsen, R. E., and Pascale, J. (1983). 'Rydberg States of Atoms and Molecules', Ch. 6 (Cambridge Univ. Press).
Komarov, I. V., Grozdanov, P. P., and Janev, R. K. (1980). *J. Phys.* B **13**, L573.
Koscher, P., *et al.* (1984). 'Lecture Notes in Physics', Vol. 213, p. 29 (Springer: Berlin).
Landau, L., and Lifshitz, E. M. (1977). 'Quantum Mechanics' (Pergamon: Oxford).
Lennard, W. N., and Cocke, C. L. (1973). *Nucl. Instrum. Methods* **110**, 137.
Lennard, W. N., Sills, R. M., and Whaling, W. (1972). *Phys. Rev.* A **6**, 884.
Pender, L. F., and Hay, H. J. (1983). *Phys. Rev. Lett.* **50**, 1907.
Powell, C. J. (1974). *Surf. Sci.* **44**, 29.
Seideman, T., Shapiro, M., and Vager, Z. (1987). *Phys. Rev.* A **35**, 87.
Sellin, I. A., Burgdörfer, J., Berry, S. D., Breinig, M., Betz, H.-D., and Groeneveld, K. O. (1986). *J. Phys.* B **19**, L155.
Sobel'man, I. I. (1972). 'Introduction to the Theory of Atomic Spectra' (Pergamon: Oxford).
Theodosiou, C. E., Inokuti, M., and Manson, S. T. (1986). *At. Data Nucl. Data Tables* **35**, 473.
Torrens, I. M. (1972). 'Interatomic Potentials' (Academic: New York).
Treacy, P. B., and Hay, H. J. (1988). 'Lecture Notes in Physics', Vol. 294, p. 136 (Springer: Berlin).
Vager, Z., Zabransky, B. J., Schneider, D., Kanter, E. P., Zhuang, G. Y., and Gemmell, D. S. (1982). *Phys. Rev. Lett.* **48**, 492.

Appendix A

In Paper III, Fig. 1 shows an energy-level diagram and decay scheme for states of a single electron into a single 2p vacancy, as occurs in the 25^+ charge state of Br. The electron may be either in a state fed from the yrast cascade $(n, \ell = n-1; n-1, \ell-1;\ \ldots\ 2, 1)$ or the direct decay $(n, \ell = 0; 2, 1)$. It was pointed out that the former's final decay, designated A2(3d to 2p), may be 'blocked', that is in such a state that the lower state cannot be reached via an electric dipole (E1) transition, simply because not all transitions can occur with the condition $\Delta m_\ell = 0$ or ± 1 satisfied, where Δm_ℓ is the change of component of ℓ in the transition.

For blocked states, non-n changing transitions 3d to 3p, 3p to 3s still can occur with, experimentally, an effective lifetime of about 90 ps. This is consistent with the theory ('Bates–Damgaard') for such transitions (Sobel'man 1972). The numerical degree of blocking, which depends on the ion's charge state (25^+ or 26^+), will be considered here in terms of the appropriate coupling schemes and quantum numbers.

(A1) States of the 25^+ Ion

In a 25^+ charge state with a single vacancy, the core, designated p^5 or p^{-1}, is in its lowest (spin–parity) $J^\pi = \frac{3}{2}^-$ state. Only an electron with this J^π may fill the vacancy, but the way in which transitions proceed depends on how states are initially fed. In high-n Rydberg states it is safe to assume that there is no preferred direction of orbital angular momentum ℓ. Also, the

Rydberg-electron's spin ($s = \frac{1}{2}$) and the core spin ($j = \frac{3}{2}$) are initially unoriented, and since we are considering E1 (non-spin) transitions, this remains true, so the use of a channel-spin notation ($S = s+j$) seems convenient.

Of the forty initial substates of the $(3d, p_{3/2}^{-1})$ configuration, only those with $J^\pi = 1^-$ may undergo E1 transitions to the 0^+ ground state. Since the initial (m_ℓ, m_s, m_j) substates are unoriented, it follows that the 15 substates of $S = 1$, and 25 of $S = 2$, are all of equal weights. The 3d to 2p transitions thus comprise 3 of $S = 1$ and 3 of $S = 2$, with a relative probability 6/40 for the A2 X-ray branch. The 3d–3p–3s transitions, which the remaining 34 substates undergo, conserve channel spins, so the final $J^\pi = 1^-$ states of the $(3s_{1/2}, p_{3/2}^{-1})$ configuration are populated by only the remaining $15-3 = 12$ substates of $S = 1$. These decay to the ground state producing the A1 X-ray and the relative probability

$$\mathrm{A1} \ : \ \mathrm{A1} + \mathrm{A2} = \frac{12}{12+6} = 0 \cdot 67$$

is obtained. The remaining 22 substates of the 3s configuration, of $J^\pi = 2^-$, are highly metastable, can decay only via magnetic quadrupole transitions, and represent the long-lived component, noted in III to display pure A1 radiation many metres downstream in a beam–foil experiment. Their lifetime is of order 1 μs (see Appendix B).

(A2) States of the 26^+ Ion

The 27^+ core of this ion belongs to the configuration p^3 which, as is well known (Condon and Shortley 1951), forms a 2^- ground state in all forms of intermediate coupling. As we shall see, this precludes formation of metastable states, and simplifies the decay scheme. Values $J \leq 5/2$ can decay to the ground 3/2 stage, so of the fifty substates, equally-populated, 24/50 can decay via 3d–2p. Since experimentally the remainder, which undergo 3d–3p–3s–2p decays, contribute X-rays of energies in the A2 range, and there are no metastable 3s states, all 26^+ double-vacancy states decay with 100% contribution to the A2 X-ray.

Appendix B: Cascade Calculations for Fits to Downstream Decays

(B1) Decay Rates

For a Rydberg state consisting of a single electron outside an ionic core, transition rates can be calculated using Gordon's (1929) equation (see Bethe and Salpeter 1957, p. 262 equations 63·2 and 63·3) for the electric dipole transitions in hydrogen-like atoms.

Tables of rates for states with (n, ℓ) up to (10, 7) are given by Bethe and Salpeter (1957); they show that the most probable decay is to the lowest available final state, i.e. $(n, \ell) \rightarrow (n' = \ell, \ell - 1)$, and that the transition strength to higher n' decreases rapidly. Hence an initial distribution over many (n, ℓ) would cascade in a few steps down to yrast states $(n', n'-1)$. In III we assumed that this pattern of 'collapse' was valid for all (n, ℓ) and used numerical extrapolation of the Bethe–Salpeter tables to obtain lifetimes and a simple approximation to branch ratios.

Subsequently, we have calculated the E1 branch transition rates $R(n', \ell'; n, \ell)$ from Gordon's equation for the range $n = 1$ to 1000, $\ell = 0$ to $n-1$. We find that the lifetimes for large n and ℓ remain proportional to $(2\ell+1)^2 n^3$, but are up to 10% higher than those deduced from the low lying states. However, for these states the most probable decay is not to the lowest available n' on the yrast line, but to the adjacent state with $n' = n-1$, $\ell' = \ell - 1$. The change between the low-ℓ and high-ℓ branch patterns is shown in Fig. 7; hence the decay sequences from states which start with $\ell \lesssim n/5$ fall rapidly to yrast states, those with $\ell \gtrsim n/5$ move parallel to the yrast line before cascading down to that line.

For our purposes, the important consequence of this is that, despite the inhibition of 'collapse', an original statistical population, weighted as $2\ell+1$, cannot feed across to the $\ell = 0$ states which decay to yield the 'C' X-rays.

(B2) Cascade Model

The time dependence of the populations of states (n, ℓ) is described by the set of coupled differential equations

$$\frac{\mathrm{d}}{\mathrm{d}t} N(n,\ell, t) = \sum_{n'\ell'} [N(n', \ell', t)\, R(n', \ell'; n, \ell) - N(n, \ell, t)\, R(n, \ell; n', \ell')],$$

where $N(n, \ell, t)$ is the number of ions in a state (n, ℓ) at time t, and $R(n', \ell'; n, \ell)$ is the transition probability between two states (n', ℓ') and (n, ℓ). Hence, from any postulated initial population $N(n, \ell, 0)$ the coupled equations can be integrated numerically to obtain the time development of the whole population. During the integration the numbers of transitions between selected pairs of levels can be extracted versus time.

This scheme has been applied to decays of Br ions according to the level scheme of Appendix A, with the Gordon rates modified where necessary to allow for the restrictions imposed by the full K shell and only one or two L vacancies in 25^+ or 26^+ ions respectively. The decays whose time development was extracted corresponded to the X-ray groups which were separated by their energies in a Si(Li) detector.

Thus, for 25^+ ions we can obtain decay rates versus time for four X-rays filling the single 2p vacancy. These are designated $A1^{25}$(s), $A1^{25}$(f), $A2^{25}$ and C^{25}, and correspond to the slow (s) M2 decay of the metastable $3s(2^-)$ state, the fast (f) E1 decay of $3s(1^-)$, transitions from 3d, and those from ns with $n > 4$. Similarly, from 26^+ ions we get two decay curves designated as $A2^{26}$ and C^{26} which corresponds to all transitions from 3s and 3d to 2p, and ns to 2p for $n > 4$.

Cascade calculations were performed for each ion charge state and each kind of initial population described in Section 2, namely, the statistical, radiative electron capture, and Landau–Zener models. The decay contributions from these were combined and fitted to the X-ray data as described below.

(B3) Combination of Cascaded Spectra

Modification of the statistical population. Most of the observed X-rays are in the A1 and A2 groups which are fed from a statistical population. The

observed decays are a combination of 25^+ and 26^+ spectra. Based on the charge-changing history of ions as they traverse the target (Hay *et al.* 1984), we assume that the fraction of ions in Rydberg states is independent of their emergent charge. Hence, cascaded 25^+ and 26^+ ion spectra can be added in proportion to the measured ion beam charge ratio $26^+/25^+ = 0 \cdot 22$. This results in close to straight-line log–log decays for the A2 and C X-rays. The observed A1 plot of Fig. 1 is curved, and results from adding the constant-slope log–log decay of $A1^{25}(f)$ to the practically constant-in-time rate of $A1^{25}(s)$. The amount of the slow component depends on the lifetime of the metastable 3s state, and a value $\tau(s) = 800$ ns matches the general curvature of A1. In A1, the 3 or 4 earliest observed points are higher than expected by comparison with the general curvature. This is due to the delay in attaining a steady population of trapped decays in the 3d–3p–3s sequence, and is accounted for by an effective lifetime near $0 \cdot 1$ ns for that sequence. Both of these lifetimes are in satisfactory agreement with estimates for the transitions involved (Paper III).

The observed X-ray decay curves (Paper I) have been re-examined using the set of Gordon transition rates and the coupled cascade relations instead of the two-branch Monte Carlo method adopted in III. For the same initial population

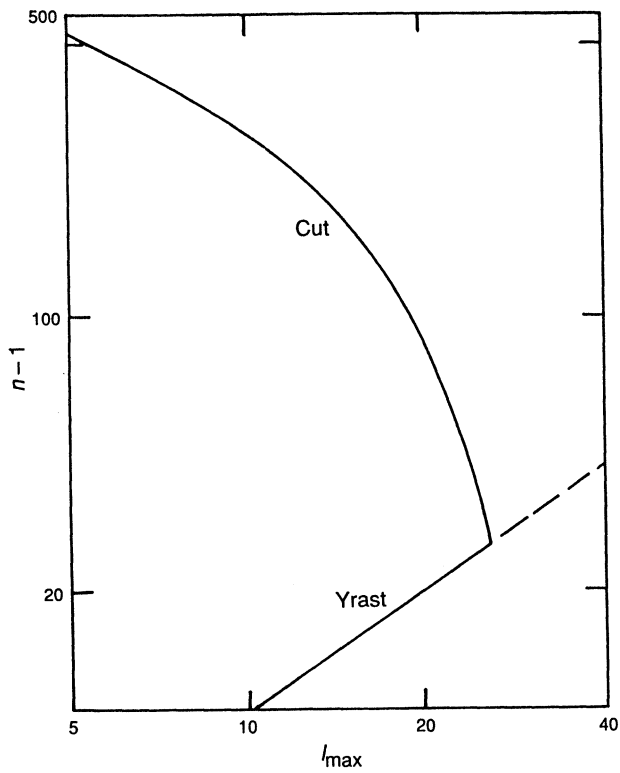

Fig. 8. Locus of ℓ_{max} versus $n-1$ for an initial n^{-3} population which best fits the data on cascading of the 'statistical' distribution. The upper solid curve 'cut' corresponds to equation (A2), meeting the 'yrast' line at $(n, \ell) = (28, 27)$. The populated states exist in the region to the left of the solid curves.

[$\rho_S(n,\ell)$ equation (1a)] we find virtually the same results, e.g. for the A X-rays $\beta = 2 \cdot 19$ (cf. $2 \cdot 14$ in III) with only a small reduction of the initial number of ions in Rydberg states due to the longer cascade path for high (n,ℓ) states.

We now discuss a fit to the data with a β value of 3. A cascade calculation with this value and with a statistical population allowing all ℓ values up to $n-1$ produces decay curves which are much too steep and have intensities far below what is observed. However, fits to the observed gradients and intensities can be obtained by modifying the ℓ distribution in the initial population: for each n, if there is a limit on the highest ℓ which is populated then the low-ℓ population is increased. This speeds up the cascade, and if the ℓ-limit decreases for higher n then the gradient of the decay curve is reduced.

An apt trial ℓ cutoff appeared to be an exponential form

$$a \exp(-b^c).$$

Values for the three parameters a, b and c were chosen by least-squares optimisation on 46 data points for the A2 and C X-rays. A tightly constrained ℓ-cutoff shape, shown in Fig. 8, was found which for $\beta = 3$, simultaneously matched the gradients of A2 and C. It also reproduced the ratio of A1 and A2 intensities, but underestimated their size; the observed intensities were recovered by making the low-n ($n \lesssim 5$) states underpopulated compared with $1/n^3$. We did not observe initial decays from $n < 10$ directly, and a reduced population for n near unity is not unexpected (Dubé and Salin 1987).

Fits obtained from an ℓ-limited statistical population for the A1 and A2 X-rays are indistinguishable from those shown in Fig. 1. Again, as in III, we find that a solely statistical population is unable to account for more than a quarter of the C X-rays.

Fits to data including all populations. Cascade spectra from REC and Landau–Zener populations have much higher fractions in the C transitions than does a statistical population. Because of its $1/n^3$ population, an REC contribution decays more rapidly than do the observed X-rays. However, the Landau–Zener population dominates the high-n Rydberg states and thus contributes more to decays seen at longer times after leaving the target.

The detailed procedure for fitting the observed X-ray decays comprises the following steps:

(1) For 100% of 25^+ ions in a statistical population, a cascade calculation gives decay curves for A1, A2 and C X-rays. Another calculation is done for 26^+ ions, and these are added in proportion to the measured charge state ratio in the total ion beam.

(2) For 100% of 25^+ ions having an REC population distribution ($1/n^3, \ell = 0$), a cascade calculation gives A1, A2 and C decay curves. Again, this is combined with a 26^+ cascade according to the REC model for the measured charge state composition.

(3) Landau–Zener 'promotions' are calculated for the electrons in 25^+ ions and the resulting population is cascaded. This is repeated for 26^+ ions and their contributions are added.

(4) The above three steps give 9 spectra. Each set of 3 has very different proportions of A1, A2 and C with very different slopes. A linear

combination of the sets is chosen by least squares criteria to give the best fit to the measured X-ray decays.

The final fit is shown in Fig. 1. The shortfall in the C X-rays from the statistical population is made up with 90% of the Landau–Zener promotion model contribution, and 6% of ions having Rydberg states following REC. If we consider the assumptions on which these models are based, these admixtures are very satisfactory.

Manuscript received 18 December 1990, accepted 26 February 1991